

# Understanding the Surface-Enhanced Raman Spectroscopy “Background”<sup>†</sup>

Sumeet Mahajan,<sup>‡,§</sup> Robin M. Cole,<sup>‡</sup> Jonathon D. Speed,<sup>§</sup> Suzanne H. Pelfrey,<sup>§</sup>  
 Andrea E. Russell,<sup>\*,§</sup> Philip N. Bartlett,<sup>§</sup> Stephen M. Barnett,<sup>‡,||</sup> and Jeremy J. Baumberg<sup>\*,‡</sup>

Nanophotonics Centre, Cavendish Laboratory, University of Cambridge, JJ Thomson Avenue,  
 Cambridge CB3 0HE, United Kingdom, School of Chemistry, University of Southampton,  
 Highfield SO17 1BJ, United Kingdom, and Scottish Universities Physics Alliance (SUPA),  
 Department of Physics, University of Strathclyde, Glasgow G4 0NG, United Kingdom

Received: July 28, 2009; Revised Manuscript Received: November 2, 2009

Even 35 years after the discovery of surface-enhanced Raman spectroscopy (SERS) much remains to be learned about the phenomenon.<sup>1–3</sup> Despite broad consensus on the mechanism of SERS, many features remain poorly understood and in particular much less effort has been put into understanding the continuum emission called the “background” observed in SERS spectra. Here the SERS background is studied systematically on sphere segment void (SSV) plasmonic substrates. We establish the physicochemical dependence of the background on plasmons, the identity of the adsorbate, adsorbate coverage and electrochemical potential. In particular, by exchanging electron-donating and electron-withdrawing adsorbates, we demonstrate predictable modulation of the SERS background. Using these observations, we propose a model for the origin of the SERS background. Finally, we test the proposed model against its predictions for anti-Stokes SERS spectra.

## 1. Introduction

A broad continuum emission called the background is always observed in SERS spectra on top of which the vibrational Raman peaks are superimposed. Vigorous investigation into the mechanism of enhancement in SERS has been carried out over the last 35 years, while related theories have been discussed trying to explain the background continuum that accompanies this SERS. Much of this discussion was confined to the initial years after the discovery of SERS. So although the SERS community is largely in consensus over the mechanism of SERS enhancement, the same cannot be said about the SERS background and its understanding. Most researchers consider it to arise either due to inelastic scattering induced by the surface roughness<sup>4,5</sup> or due to luminescence<sup>6</sup> due to the molecule. In 1980 Furtak and Reyes published a critical review of the proposed theoretical models of the SERS background.<sup>7</sup> Among the most prominent theories of that time, those by Gersten et al.<sup>8</sup> (GBL model) and Burstein et al.<sup>9</sup> (BCCLT model) stand out. The key features of these two models are illustrated in Figure 1. In the GBL model, the electronic coupling of the upper LUMO state of the molecule with the metal broadens the HOMO–LUMO transition, so that photoexcitation in the molecule becomes possible and is followed by a rapid tunneling of the photoexcited electron into the metal (curved dashed line on the metal side of Figure 1a). Such tunneling requires close proximity of the molecule to the metal. In contrast, the BCCLT model depends generally on single-particle electron–hole pair transitions enhanced at rough metal surfaces, with Raman relaxation of the excited electron followed by subsequent re-emission producing the background (Figure 1b) alongside the “giant” Raman scattering. Nevertheless, all of the existing theories still fall short of providing a

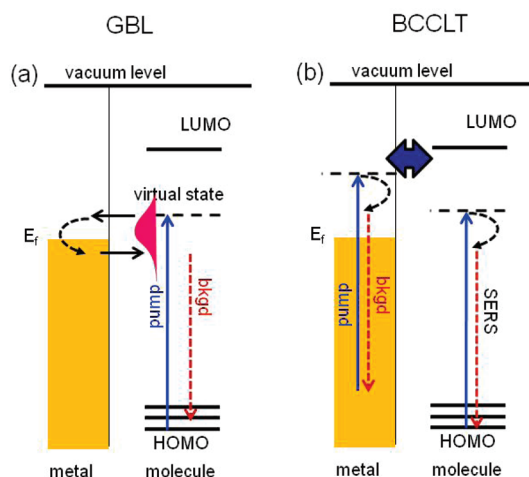


**Figure 1.** Schematic of the (a) GBL<sup>8</sup> and (b) BCCLT<sup>9</sup> models illustrating the generation of the “background” in a SERS process. In (a), “virtual” photoexcited HOMO electrons can tunnel into the metal before tunneling back out after relaxation due to the charge transfer. In (b), the LUMO level couples to the empty metal states (blue arrow). Photoexcitation of metal electron–hole pairs at rough metal is followed by relaxation and re-emission.

comprehensive explanation of all the observations by various researchers.<sup>10</sup> A brief summary of further developments in understanding regarding the observed continuum has been provided by Moskovits in his reviews on SERS.<sup>11,12</sup> Recently, it has also been suggested that the continuum observed in SERS might be related to plasmon coupled emission.<sup>13,14</sup> Another study suggests that emission features may arise due to inelastic scattering of “hot” electrons or may be enhanced fluorescence.<sup>15</sup> In the past decade SERS research has been dominated by the quest for the greatest SERS enhancements and the exploration of applications of SERS, which has often prompted researchers to largely ignore the background and to resort to the use of background subtraction methods, the details of which are not always reported. It also appears that a large section of the SERS

<sup>†</sup> Part of the “Martin Moskovits Festschrift”.

\* Corresponding author. E-mail: J.J.B., jjb12@cam.ac.uk; A.E.R., aer1@soton.ac.uk.

<sup>‡</sup> University of Cambridge.

<sup>§</sup> University of Southampton.

<sup>||</sup> University of Strathclyde.

community believe that the background arises from carbonaceous contaminants burned onto the sample surfaces from high levels of laser irradiation, which may indeed be the case in some circumstances but is not thought to be the generally applicable source of the background. Thus, a comprehensive understanding of the mechanism of the background emission is still very much awaited.

Understanding the background is essential to provide the means to obtain improved SERS substrates with better sensitivities and faster measurements. In general, the enhanced SERS peaks are accompanied by enhanced backgrounds, thus limiting improvements in signal-to-noise and detection of weak transitions. Similar to the case of the enhancement mechanism, irreproducibility of substrates has also been a deterrent for systematically understanding the continuum observed in SERS. Over the past several years our group has led the development of colloidal crystal templated electrodeposited substrates.<sup>16–18</sup> These structured nanovoid surfaces, called sphere segment void (SSV) substrates, show reproducible SERS<sup>16–19</sup> and surface-enhanced resonance Raman scattering (SERRS)<sup>20</sup> with enhancements of the order of  $\sim 10^6$  and  $\sim 10^8$ , respectively, on gold substrates. These have also been well studied in electrochemical SERS applications.<sup>21–23</sup> The SERS enhancement properties correlate well with plasmonic absorptions on these substrates and a fair understanding of the plasmon modes on these surfaces has been achieved.<sup>16,24–26</sup> Hence, SSV substrates provide the ideal SERS platforms for systematically studying the background and its mechanism.

In this paper we report results on the SERS background as observed on SSV substrates. We show the correlation of the intensity with the strength of plasmons on SSV substrates. By choosing a set of para-substituted thiophenols and systematically studying their exchange in solution, we show that the background observed in SERS is dependent on the nature of the molecule adsorbed on the surface and changes in consonance with the intensity of peaks. The modulation of the intensity of the background maximum is observed to vary as a function of the electrode potential of SSV substrates. Thus, we show that there are undoubtedly electromagnetic and chemical contributions to the generation of the background. Utilizing these observations, we suggest an image-molecule-mediated coupling to electronic excitations in the metal as the origin of this background. Finally, the model is tested against results obtained for anti-Stokes SERS observed on SSV substrates. Our results clearly show the systematic origin of the background and exclude contaminant explanations.

## 2. Experimental Section

**2.1. Fabrication.** SSV substrates were prepared in a two stage process, employing self-assembly and electrodeposition as shown schematically in Figure 2. Substrates for templated electrodeposition were prepared by evaporating 10 nm of chromium followed by 200 nm of gold onto 1 mm thick glass microscope slides. These substrates were extensively cleaned by sonication in 2-propanol, followed by rinsing in deionized water and dried using argon. These were then dipped in a 10 mM ethanolic solution of cysteamine for at least 48 h. Colloidal polystyrene spheres were obtained as 1 wt % aqueous suspensions from Duke Scientific Corp. The self-assembly of colloidal spheres was carried out in a thin layer cell composed of the cysteamine-coated gold surface and a clean, uncoated microscope cover glass held 100  $\mu\text{m}$  apart by a spacer cut from Parafilm (Pechiney Plastic Packaging, Inc.). Slow evaporation at controlled temperature resulted in an opalescent ordered

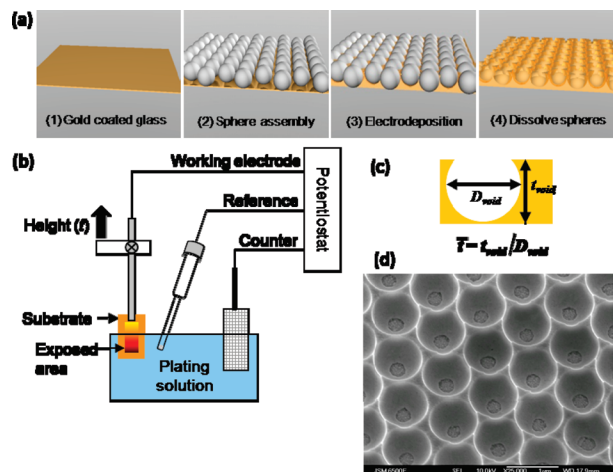


**Figure 2.** (a) Schematic of self-assembly and electrodeposition procedure for fabricating SSV substrates. (b) Schematic of the electrochemical setup for preparing graded substrates. Working electrode and substrate are progressively withdrawn to obtain a sample with a gradation of thicknesses, with the thinnest film at the top and thickest at the bottom of the sample. A delimited rectangular area of the template is left exposed while masking the remaining area with an insulating varnish. A saturated calomel electrode is used as the reference and a platinum mesh as the counter. (c) Definition of normalized thickness,  $\bar{T}$ . (d) Typical SEM image of a gold SSV substrate (scale bar: 1  $\mu\text{m}$ ). Note that the smaller diameter holes at the bottom of each void arise from contact between the latex spheres and the evaporated gold coated glass slide.

monolayer of spheres, which served as a template for electrodeposition. The electrochemical deposition was performed in a separate thermostated cell at room temperature using a conventional three-electrode configuration controlled by an Autolab PGSTAT30. The template-coated gold substrate was the working electrode with a large area platinum gauze counter electrode and a homemade saturated calomel reference electrode in the electroplating step. Gold was deposited from a commercial cyanide-free gold plating solution (ECF 60, Metalor). A plating additive (Brightener E3, Metalor) was added to the plating solution to give a smooth finish to the deposits. Silver was deposited from cyanide free commercial plating solution obtained from Technic UK (LEKTRACHEM Ltd.). Electroplating was carried out under potentiostatic conditions against a homemade mercury/mercurous sulfate reference electrode (MSE), at a potential of  $-0.125$  V vs MSE. For studying the plasmon spectral dependence, samples with a series of steps in SSV thickness (referred to as a graded sample) were fabricated, according to the scheme shown in Figure 2b. This allowed the systematic study of plasmons and SERS as a function of structure morphology on a single substrate. A rectangular area of the structure was exposed by masking the rest of the template with an insulating varnish. A precalculated charge was passed through the template to obtain a particular thickness of gold in a potentiostatic electrodeposition pulse at  $-0.73$  V versus a saturated calomel electrode (SCE) as reference. The template was withdrawn from the electroplating solution in 1 mm steps and the differential charge corresponding to the new thickness was passed. In this way a sample with a systematic gradation of thicknesses was obtained, with the thinnest film at the top and the thickest at the bottom. After electrodeposition, the polymer spheres were removed by dissolving in DMF. This resulted in substrates with an array of interconnected spherical cavities, shown in Figure 2a. For other studies a uniform thickness SSV substrate was prepared by passing a precalculated

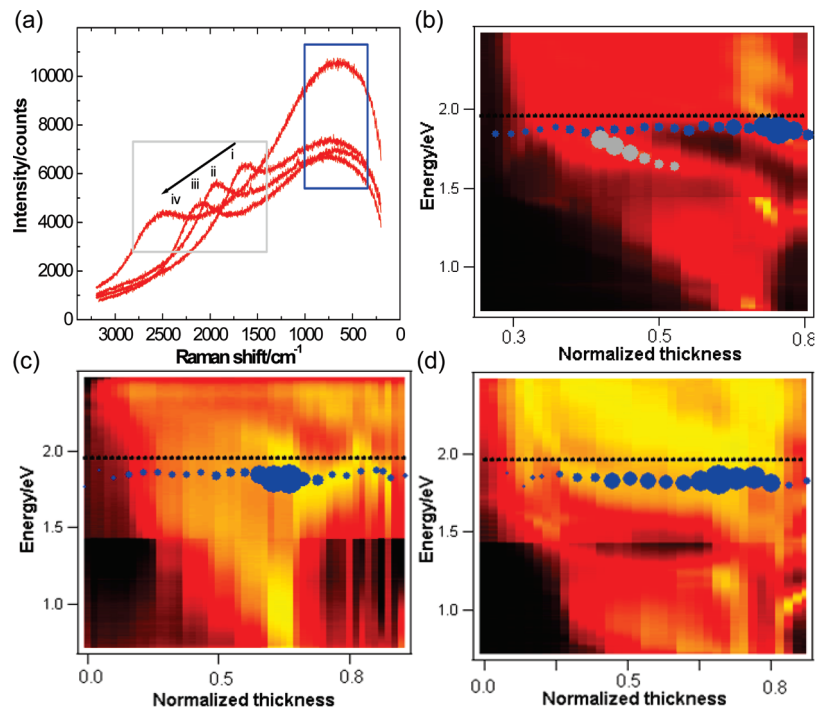


**Figure 3.** (a) Features in the background shown for a series of spectra recorded at increasing film heights (i–iv;  $\bar{t} = 0.4$ – $0.5$ ) on a 600 nm sphere templated gold SSV substrate. The broad maximum discussed in the text is indicated by the blue box and the smaller film height dependent feature by the gray box. The positions of the overall maximum of the background (blue) and that of the smaller feature (gray) are overlaid on the plasmon maps for (b) 600, (c) 400, and (d) 800 nm sphere templated graded gold SSV substrates. The diameter of the blue circles is proportional to the intensity of the overall background maximum and is comparable between the three maps. The gray circles represent the position and relative intensity of the smaller feature observed in the background in (a). The black dashed line represents the laser excitation at 633 nm.

fixed amount of charge in a single electroplating step (with geometry confirmed by electron microscopy).

**2.2. SERS Measurements.** Spectra with a 633 nm laser were acquired on a Renishaw 2000 Raman microscope system. Spectra with the 785 nm laser were recorded in the kinetic mode with a Perkin-Elmer 400S RamanStation. Stokes and anti-Stokes spectra with a 785 nm laser were also recorded using a Renishaw 1000 Raman microscope system equipped with a holographic supernotch filter. The peak intensities reported in this paper have been calculated after subtracting the background from the spectra and curve-fitting using cubic spline interpolation using Spectrum 2.0 and Wire 9.0 software. The intensity of the background used for plotting graphs is the absolute intensity at a fixed wavenumber or the maximum obtained after curve-fitting to the broad “background” spectrum disregarding the SERS peaks.

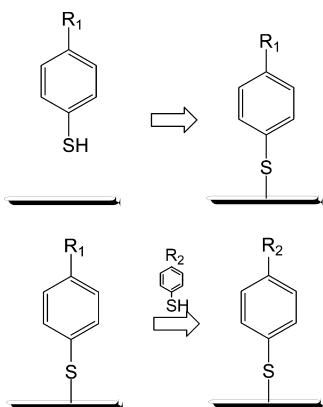
**2.3. Plasmon Maps.** Broad-band reflection spectra were measured for a range of incident angles in a purpose-built goniometer, at selected positions across the graded SSV samples.<sup>16,24–26</sup> Dips in the reflectivity correspond to plasmonic absorption (up to 100%, plotted in yellow on the color scale images), and maps are constructed tracking these resonant plasmon absorptions as the morphology of the SSV substrates changes across the sample.

### 3. Results and Discussion

**3.1. Plasmon Dependence.** In all SERS spectra the peaks ride on a broad continuum, which is called the “background”. The shape of this depends on the substrate, although it is usually featureless with a broad maximum. However, on SSV substrates this broad maximum often shows some smaller features. These smaller features were found to vary systematically with thickness of the SSV substrates. The SERS spectra in Figure 3a show such a typical feature on a 600 nm sphere templated gold

substrate in the presence of an adsorbed monolayer of benzenethiol. In this case, the background intensity dwarfs the SERS peaks, which are hardly visible in the spectra, for this specific sample morphology. The position of the overall maximum of the broad feature remains nearly the same, while the position of the smaller feature shows a red shift (higher Stokes-shifted wavenumber) with increasing film-height. The absolute intensities at the position of the maximum and the smaller feature were found to be linearly dependent on laser power. This confirms that the background emission is certainly not due to two photon processes such as second harmonic generation or two-photon excited photoluminescence, as these would cause the background to be nonlinearly dependent on incident laser power.

As mentioned above, some of the features on the background were observed to vary systematically with the film height of SSV substrates. This prompted us to investigate their dependence on the plasmonic absorption of the substrate, as the plasmons have also been shown to vary systematically with the thickness of SSV films.<sup>25,26</sup> The position of the overall maximum as well as that of any smaller features observed were extracted from the SERS spectra and overlaid on the plasmon maps of the respective substrates. Results are shown for graded gold substrates templated with 400, 600, and 800 nm spheres in Figure 3c,b,d. The corresponding relative intensities are indicated by the diameter of the circle plotted for each point. It is clear that both the position of the broad maximum and that of the smaller feature (when present) are closely related to the dispersion of plasmon modes across the thickness of the substrates. This is especially true for the smaller feature, which coincides closely with one of the specific localized plasmon modes. We note that the position of the broad maximum is always red-shifted by a similar magnitude compared to the laser excitation energy. Significantly, the background shows a distinct

**SCHEME 1: Scheme for Studying the Adsorption of Thiols and Their Exchange on SSV Substrates**

enhancement at the same locations as strong plasmonic absorptions that match either the laser excitation or the emitted radiation. Moreover, this enhancement profile is almost exactly the same as that observed for the SERS peaks.<sup>24</sup> Further, the red shift of the main broad background feature with respect to the laser line suggests a nonradiative loss in energy. The slight variability in the position of the maximum and the breadth of the peak suggests the involvement of the metal, rather than the molecule, because the metal has a continuum of states rather than discrete levels such as in a molecule, which in any case possesses no transitions at these energies. Nevertheless, the strong correlation of the background intensity with SERS points to a coupled or codependent process.

Furthermore, in previous near-infrared (NIR) SERS experiments using SSV substrates and 1064 nm excitation, which is well clear of electronic resonance with the adsorbate, a strong background continuum was still observed. With less enhancement of the background than for 633 nm excitation, this yielded a higher signal-to-noise ratio using excitation at 1064 nm.<sup>18</sup> In these NIR SERS experiments the highest background and SERS peaks were also found to be coincident with strong plasmonic absorption, once again illustrating correlation of the two processes.

**3.2. Chemical Dependence.** To establish the correlation of the background with adsorption of molecules on SSV substrates, a system of thiol adsorption and exchange shown in Scheme 1 was chosen because of its simplicity and the well-defined spectra of the molecules. The scheme was used for monitoring the adsorption of thiols (top) and their exchange (bottom). This allowed the study of the effect of adsorption of molecules and the nature of substituent (R<sub>1</sub> and R<sub>2</sub>) on the background.

The effect of increasing coverage of the adsorbate, benzenethiol, was systematically studied by recording SERS spectra as follows: the SERS substrate was soaked in 10 mM benzenethiol solution for a specified time, taken out, immediately rinsed thoroughly with copious amounts of ethanol, and dried under nitrogen, and the spectrum was recorded in air, and the spectrum was recorded. The substrate was then returned to the solution to increase the coverage, and the procedure repeated. The SERS spectra as a function of exposure time are shown in Figure 4. As seen in Figure 4, both the SERS peaks of benzenethiol and the background show a gradual systematic increase. The inset in Figure 4 shows the evolution of the height of the 1572 cm<sup>-1</sup> SERS peak and the absolute intensity of the background at 2750 cm<sup>-1</sup> with time. The increase in the intensity of the background mirrors that of the SERS peak, with both saturating at longer times, which may be indicative of the

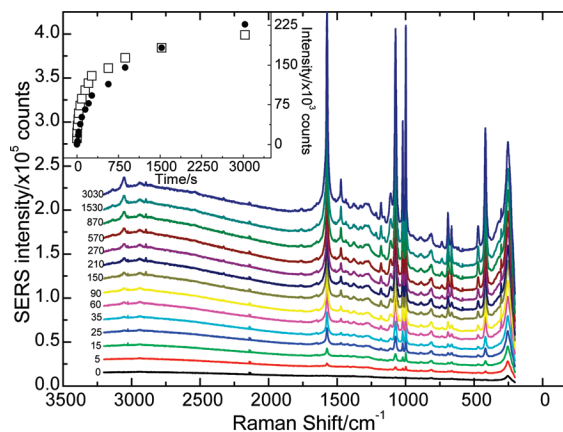


**Figure 4.** SERS spectra recorded on a  $D = 600$  nm,  $\bar{t} = 0.7$  silver SSV substrate after soaking the substrate in an ethanolic 10 mM benzenethiol solution. The immersion times (s) are indicated for each spectrum. After the specified time, the substrate was washed with ethanol and dried under a stream of nitrogen. Spectra recorded with a 633 nm laser at 3 mW laser power with a single scan of 10 s. The spectra are *NOT* offset from each other. Inset: extracted peak height of the 1572 cm<sup>-1</sup> benzenethiol peak (squares) and the absolute intensity of the background at 2750 cm<sup>-1</sup> (circles).

formation of a complete monolayer. It should be noted that a small background signal was present in the spectrum obtained prior to exposure to the benzenethiol solution (time = 0 s in Figure 4), but a much larger background is observed upon adsorption of the molecule under investigation.

To gain further insight, with added control, similar adsorption experiments were carried out in solution, i.e., investigating the formation of the monolayer in the solution cell without periodically removing the sample, using three para-substituted benzenethiols: *p*-methoxybenzenethiol (MBT), *p*-nitrobenzenethiol (NBT), and *p*-carboxybenzenethiol (CBT). In such solution studies the background showed either a monotonic increase or decrease as a function of time/coverage depending on the molecule chosen, and this change is concomitant with the change in the intensity of SERS peaks. Note that in air only an increase in intensity is observed on adsorption of molecules compared with the substrate having no “deliberately” adsorbed molecules. These experimental results demonstrate that the background is correlated with the SERS response as also found by other researchers.<sup>27,28</sup> However, our results also point out that there is a more subtle phenomenon at play, which depends on the nature of the molecules adsorbed on the surface.

To unravel the complexities of this molecular dependence, we studied the exchange of the aforementioned para-substituted thiols in solution. Interpretation of the variation in the background is more reliable in this case, as the experiment is always conducted with a well-defined interface and the molecular displacement is with a structurally similar molecule, which differs only in the terminal functional group. Hence, the first thiol was adsorbed on a gold SSV substrate by exposure to the ethanolic 10 mM solution for at least 2 h. Thereafter, the exchange experiments were carried out in a SERS cell,<sup>1</sup> in which a thin layer of solution is trapped between the substrate (which is mounted on the end of a movable shaft) and the optical window. The cell was filled with a fixed volume (30 mL) of deionized water. The surface replacement was initiated by introducing 100  $\mu$ L of a 30 mM thiol aqueous or ethanolic solution, as defined by the solubility of the thiol at a distance of  $\sim 5$  cm behind the surface, thus allowing the molecules to slowly diffuse toward the surface where the exchange then

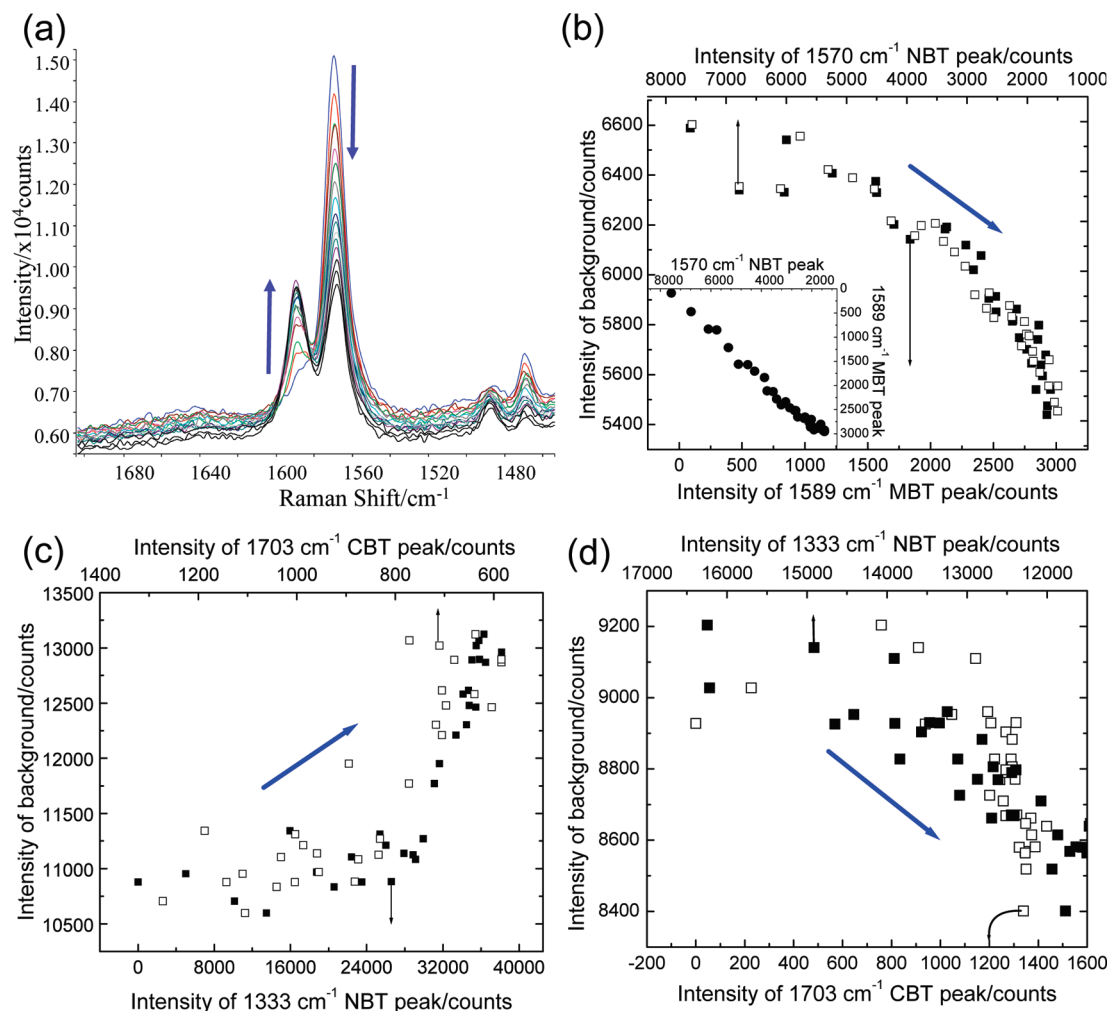


**Figure 5.** (a) SERS obtained on 600 nm,  $\bar{\tau} = 0.8$  gold SSV substrates recorded every 30 s for exchange of adsorbed *p*-nitrobenzenethiol (NBT) by *p*-methoxybenzenethiol (MBT) in water. Laser: 785 nm, 100 mW, 10 accumulations of 1 s exposure. The blue arrow indicates the progress of the experiment beginning at time = 0 in all the plots. (b) Background intensity plotted versus the increasing MBT (filled squares) and decreasing NBT (open squares) peak intensities for the spectra shown in (a). The inset shows the plot of NBT versus MBT peak intensity. (c) and (d) Background intensity plotted as for (b) for (c) replacement of *p*-carboxybenzenethiol (CBT) covered surface (open squares) by NBT (filled squares) and (d) replacement of NBT (open squares) covered surface by CBT (filled squares).

occurred, while spectra were acquired in the kinetic mode every 30 s. These concentrations and geometry were found to work best as they slowed down the displacement process. A representative set of spectra acquired with this methodology are shown in Figure 5a for the exchange of the adsorbed *p*-nitrobenzenethiol (NBT) by *p*-methoxybenzenethiol (MBT) on a gold SSV substrate. Note that the background has not been removed from the spectra and is apparent as the offset of the baseline of the spectra to  $\sim 6000$  counts. As the exchange occurred, the intensity of the peak at 1570  $\text{cm}^{-1}$ , attributed to the  $\nu_{\text{C-C}}$  ring mode of NBT, and the background measured at 1520  $\text{cm}^{-1}$  (well clear of the peaks) decreased, while the peak at 1589  $\text{cm}^{-1}$ , assigned to the  $\nu_{\text{C-C}}$  ring mode of MBT increased. The intensity of the background is plotted vs the extracted intensities of the NBT (top *x*-axis, decreasing left to right) and MBT (bottom *x*-axis, increasing left to right) peaks in Figure 5b. The inset in Figure 5b shows the plot of the NBT peak versus the MBT peak, which appears almost linear, indicating a one-to-one displacement exchange between the two thiols.<sup>29,30</sup> It is noted that the only difference between the two molecules in this case is the nature of their para substituent, which is electron donating in the case of methoxybenzenethiol and electron withdrawing for nitrobenzenethiol. Hence the results suggest that the background depends on the electronic structure

of the molecule and its resulting interaction with the metal surface as well as being dependent on both plasmons and adsorbate coverage.

The effects of the electron withdrawing or donating nature of the adsorbate molecule on the background, was tested further by using NBT and *p*-carboxybenzenethiol (CBT). Again we note that the carboxy substituent is electron-donating in nature compared to the nitro group. Equilibrium between both species on the surface was attained from different starting points in Figure 5c,d. In Figure 5c the substrate is initially coated with CBT and, thereafter, the displacement reaction is carried out with NBT. In Figure 5d NBT is first chemisorbed on the surface and then an exchange reaction is carried out with CBT. Thus, in Figure 5c it can be seen that the CBT peak intensity decreases while the NBT peak intensity increases as the reaction progresses and this is accompanied by an increase in the background intensity. On reversing the conditions, the opposite happens, as evident from Figure 5d. Together the results shown in Figure 5 suggest a role of the local charge distribution at the surface produced by different adsorbate molecules in determining the SERS background.

Changing the applied electrode potential also results in a variation in the strength of the electric field at the interface (across the adsorbed molecule). Thus, it is expected that the

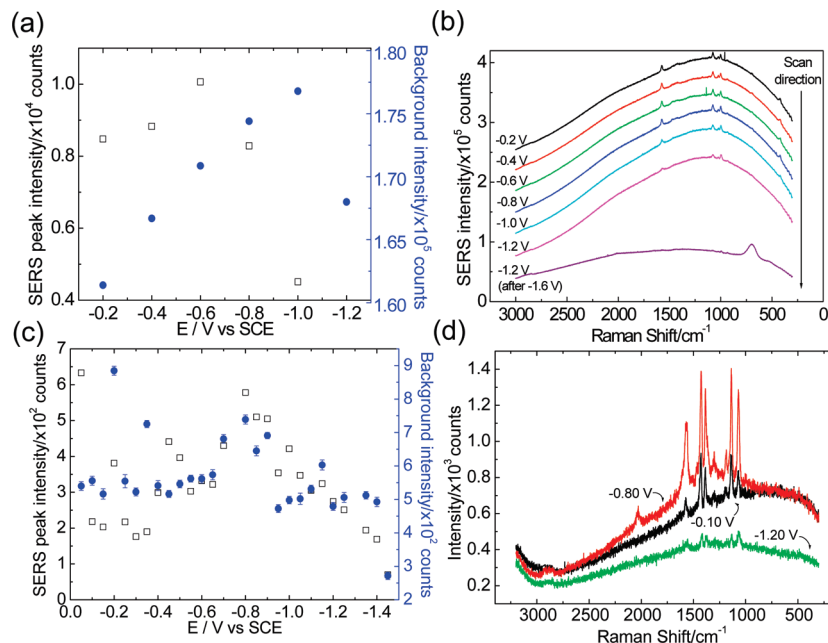


**Figure 6.** SERS obtained on 600 nm,  $\bar{r} = 0.75$  gold SSV substrates. (a) Intensity of pyridine peak and background maximum during electrochemical stripping. (b) Spectra of benzenethiol during electrochemical stripping. (c) Intensity of benzenethiol and background maximum during electrochemical stripping. (d) Spectra of pyridine at a potential of zero charge ( $-0.10$  V), at maximum intensity ( $-0.80$  V), and at stripped potential ( $-1.20$  V).

SERS background intensity will be dependent on the applied electrochemical potential, and this was investigated by monitoring the bias-dependent SERS for monolayers of benzenethiol and pyridine adsorbed on SSV gold surfaces. The spectra of an adsorbed benzenethiol monolayer obtained in situ in an aqueous solution of  $0.1$  M  $\text{NaClO}_4$  are shown in Figure 6b and the corresponding SERS peak height of the ring mode ( $\nu_{\text{C-C}}$ ) at  $1572$   $\text{cm}^{-1}$  and the background intensity measured at  $1750$   $\text{cm}^{-1}$  in Figure 6a. As the potential was made increasingly negative, resulting in an increase in the electric field strength (in  $0.2$  V steps, starting from  $-0.2$  to  $-0.8$  V vs SCE), the intensity of both the peak and background increased. At potentials below  $-0.8$  V, adsorbed benzenethiol is gradually reductively desorbed from the surface. After the potential is held at  $-1.6$  V for a few minutes, the benzenethiol peak is no longer present in the spectrum obtained at  $-1.2$  V. This is accompanied by a significant change in both the magnitude and the shape of the background. The corresponding bias-dependent spectra obtained for stripping a pyridine monolayer in  $\text{NaClO}_4$  are shown in Figure 6d. Once again, the intensity of the SERS peaks and the background increased as the potential was made more negative up to  $-0.8$  V, where stripping of the monolayer began. Such an increase in the SERS intensity with increasingly negative potential has been previously reported for pyridine and pyrazine adsorbed on an unroughened Au(210) electrode by Brolo et al.<sup>31</sup> By using such a well-characterized surface, they were able to demonstrate that the increase in intensity was not accompanied by a change in coverage or orientation of pyridine over the potential range covered in our experiment presented in Figure 6c,d and were thus forced to conclude that no simple relationship could be found between SERS intensities and surface coverage for surface concentrations close to one monolayer. Once again there appears to be a more subtle phenomenon involved, which will be discussed in the context of the model proposed below.

### 3.3. Model for Background Mechanism and Discussion.

A model (Figure 7) is now proposed to account for the background observed in SERS experiments, based on the experimental evidence presented above. The essential constraints of the model are that the background is not dependent on

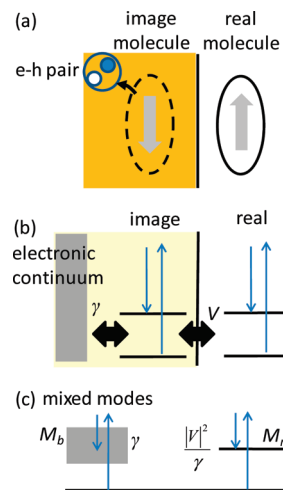


**Figure 7.** Image molecule model for the generation of the background in SERS. (a) Plasmonic excitation of the molecule generates transient dipoles that excite real and image molecules, which in turn are coupled to electron-hole pairs in the metal. (b) Raman transitions of real and image molecules are differently coupled to the continuum. (c) Resulting normal modes have very different line widths, giving rise to the continuum and SERS peaks.

electronic mixing of the adsorbate molecule with the surface but instead involves Coulomb-coupled excitation of electrons in the metal by the surface plasmons excited by the nonresonant laser. We present here the model for the case of a near-perfect metal (hence we use an image charge formalism) and defer our full quantum mechanical theory to a separate publication. The transient dipoles created by the vibrating molecule are thus mirrored by equivalent displacements of the image charge distribution within the metal. We present the argument here for dipoles aligned parallel to the surface, though it proceeds in similar fashion for perpendicularly aligned dipoles, and we defer also discussion of selection rules (which in any case are mixed on our nanostructured substrates). Although electronic Raman scattering of metals has been calculated for delocalized electrons (which couple extremely poorly to incident photons or plas-

mons), here the image dipole inside the metal acts as a point source which couples to free electronic states. This causes strong damping,  $\gamma$ , of the charge oscillations in the mirror molecule, and thus indirectly to the plasmon-excited real molecule outside the metal. The coupling,  $V \ll \gamma$ , between real and image molecules is by dipole–dipole coupling (renormalized by the effective dielectric constants). Plasmons excite both the real and image molecules in specific superpositions, and two normal modes,  $M_b$  and  $M_r$ , of the coupled system are seen to dominate the response. The first normal mode,  $M_b$ , is a rapid coupling to the electronic metal states, and this component gives rise to the broad background, while the second normal mode,  $M_r$ , arises from a superposition of real and image molecular dipoles that leaks slowly into the metal and provides the sharp Raman transitions normally found in SERS.

A simple way to visualize these different SERS components is that the laser-excited plasmons either excite the real molecule (giving the SERS peaks, now broadened by Coulomb coupling via the image molecule to the electronic continuum) or excite the image molecule (giving equivalent SERS peaks that are drastically broadened into a background by the strong coupling to the electronic continuum). An approximate theoretical analysis of this situation gives for the Stokes intensity,

$$S_{\text{Stokes}}(\omega) = 2\gamma[\bar{n}(\nu) + 1] \left[ \frac{\gamma^2 \eta^2}{(\omega - \omega_l + \nu)^2 + \gamma^2} + \frac{|V|^2}{(\omega - \omega_l + \nu)^2 + |V|^4/\gamma^2} \right] \quad (1)$$

with the normal definition of the thermal occupation of vibrational states,  $\bar{n}$ , and the strength of the image dipole  $\eta = |[\epsilon(\nu) - 1]/[\epsilon(\nu) + 1]|$  being dependent on the dielectric constant at the Stokes frequency. The first term in (1) corresponds to the background while the second term, which is resonant around  $\omega_l - \omega = \nu$ , gives the narrow SERS peaks. This model is also sensitive to the local electronic environment through  $\epsilon(\nu)$ , implying the ability to tune the background SERS strength through the effective dielectric constant modified by molecules attached to the surface. The strength of the Coulomb coupling between the dipole and its image,  $V$ , depends on the  $z^{-3}$  falloff of the dipole–dipole coupling with separation from the surface,  $z$ , and this thus controls both the SERS peak and the background.

The mechanism of background generation from our model is closest to but yet distinct from those proposed by Burstein et al.<sup>9</sup> (see Figure 1). In our model it is the image molecule that locally excites e–h pairs (or excitons) in the metal, which is not clearly proposed in the mechanism of Burstein et al. Moreover, our model has an explicit role for plasmons, which the BCCLT model<sup>9</sup> does not take into account. Above all, the model is able to account for all the observations on SSV substrates as now discussed below.

This model explains the enhancement of the background emission by plasmon modes, since the larger optical coupling produced by high surface plasmon optical fields at the surface results in enhanced coupling to both the real and image molecules. In fact, the plasmon boundary conditions indicate that the real and image molecules must be excited in a specific superposition. Similarly, the photon re-emitted after scattering radiates more efficiently if a plasmon mode exists at that frequency, explaining the appearance of the smaller features in the overall broad continuum of the background as observed in Figure 2. Without plasmons present, for instance on equivalent SSV nickel surfaces, no background emission (or SERS) is seen. The spectral width of the background (discussed further below)

and its maximum spectral position arises from the various factors including the thermal phonon occupation, the density of states for electronic excitations, and the degree of localization of the image molecule charge distribution (which changes the strength of coupling to the electronic continuum). The observation of a background in SERS even with near-infrared radiation on such plasmonic substrates is thus accounted for by the generation of electron–hole pairs inside the metal. The proposed model successfully accounts for why the background and SERS occur concurrently, since they are both enhanced by plasmons and the proximity of the molecules to the surface. The model provides a mechanism for how species at the interface can affect the electric field at the metal surface. Electron withdrawing molecules pull electrons from the metal closer to the surface molecules, reducing the dielectric screening and increasing the background emission. Similar electron-donating molecules suppress this dipole–dipole coupling to the image molecule. More generally, an increase or decrease in the background will depend on the nature of molecules being displaced and their interaction with each other and the surface, as confirmed by our observations. In addition, our model suggests how the background is altered through electrochemical potential or ionic species at the interface. The modulation of electrochemical potential modifies the double layer at the surface, again changing the local dielectric screening. This effect of electrochemical modulation of potential on the background observed in SERS has been studied earlier on silver electrodes<sup>32</sup> and is also consistent with our proposed model.

**3.4. Anti-Stokes SERS.** So far only Stokes scattered SERS results have been presented and the image molecule–electronic continuum model has been found to at least qualitatively explain the observations. Therefore, it is pertinent to test the model from the perspective of anti-Stokes SERS. Since the background continuum is generated by electronic electron–hole pair excitation, the anti-Stokes spectrum will depend on the thermal occupation of this continuum. This was verified by investigating benzenethiol and pyridinethiol adsorption on gold SSV substrates with similar morphologies ( $D = 600$  nm,  $\bar{r} = 0.8$ ). The Stokes and anti-Stokes spectra are presented in Figure 8, and indeed, no equivalent background is found on comparing similar wavenumber regions of the respective spectra. We note that the anti-Stokes background was found to vary linearly with laser intensity, eliminating the need to consider contributions from laser heating. The rising background toward lower wavenumbers in the anti-Stokes spectra has virtually no contribution from laser scatter (which may get through the notch filter, and is separately observed in the bulk Raman spectra of benzenethiol). Instead, this anti-Stokes background reflects the exponentially small probability of extracting energy from hot electron–hole pairs in the metal. The exponential falloff in this tail with a  $1/e$  anti-Stokes Raman shift of  $200$   $\text{cm}^{-1}$  corresponds reasonably to the thermal energy  $k_b T = 25$  meV. The background and SERS peak intensities depend on the specific molecule, as illustrated by comparing (a) and (b) of Figure 8, but the shape of the background spectrum is governed by the metallic nanostructure. Not only are the peaks more intense for benzenethiol compared to pyridinethiol, but also the ratios between the corresponding Stokes and anti-Stokes peaks are higher in the former molecule than the latter, with a ratio of 20–40 being found for pyridinethiol and 10–500 for benzenethiol. In particular, for the pyridine peak at  $1000$   $\text{cm}^{-1}$  the Stokes to anti-Stokes ratio is 40 while for the benzenethiol peak at  $998$   $\text{cm}^{-1}$  the ratio is 83. For the same thermal distributions of electrons and holes in the metal, the different molecules give different charge distribu-

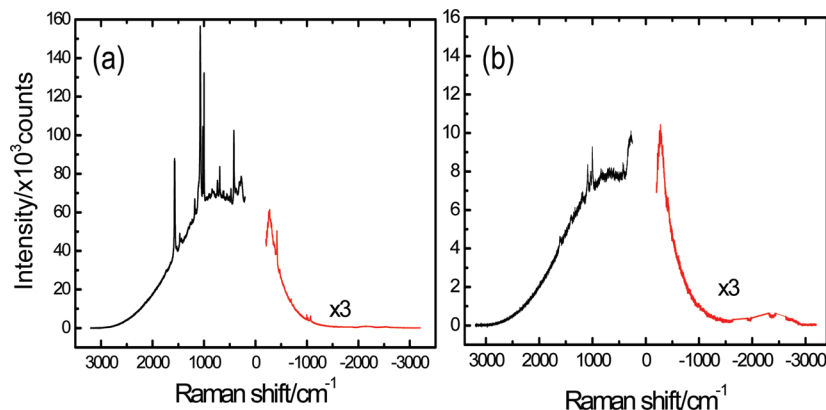


**Figure 8.** Anti-Stokes and Stokes spectra of benzenethiol (left) and pyridinethiol (right) recorded with a 785 nm laser. Spectral acquisition time: 10 s in all cases; laser power 5.8 mW at the sample. The anti-Stokes spectra are multiplied by a factor of 3 to aid the comparison.

tions (which influences  $\varepsilon(\nu)$ ) and different spatial localization (which controls  $\gamma$ ). This yields a background emission in the case of pyridinethiol that is 10 times weaker than for benzenethiol. Interestingly, even less SERS is seen for the pyridinethiol, showing that the ratio of SERS to background is not entirely fixed, but modified by the relative rates of Coulomb coupling between image- and real-molecules and the strength of coupling to the electronic continuum. The absence of a significant background continuum emission on the anti-Stokes side proves it originates from the electronic continuum in the metal and validates our proposed model.

Thus we have put forward a model mechanism that explains the origin of the background and is able to explain all our observations. Nevertheless, it makes other predictions that need to be tested further. Among those that would be interesting to study are the molecule–metal distance dependence of the SERS background in comparison to the SERS peaks, confirming how these may arise from similar mechanisms, and this work is currently in progress. Another prediction made by our model is that control of the surface curvature can affect the size of the image dipole, and hence how strongly it can couple to the electronic continuum.

#### 4. Conclusion

In this paper we have reported an extended study of SERS spectra on SSV plasmonically engineered substrates aiming to decipher the generation mechanism of the background emission. The plasmon dependence of the background in SERS spectra is clearly demonstrated, while the effect of molecules is substantially resolved. It is demonstrated that this continuum emission is strongly correlated with adsorption of molecules on SERS substrates and depends on the nature of the molecule as well: the background is thus dependent on both the metal and the molecule. The observation of background emission with NIR laser excitation proves that it is not just plasmon enhanced luminescence from the molecule. Thiol exchange experiments show that electron donation decreases the background while electron withdrawal increases the background. Similar conclusions are found on varying electrochemical potentials. Using these observations, an image-molecule/electronic continuum coupling model has been proposed to explain the origin of the background observed in SERS. The model proposes a dipole–dipole coupling between real and image molecules that provides an additional Raman scattering with electron–hole pairs in the metal to generate the background. This model was tested against the prediction of the background in anti-Stokes SERS

spectra and indeed no continuum emission is found compared to the Stokes spectrum.

**Acknowledgment.** We acknowledge useful contributions of Mamdouh Abdelsalam and Patrick J. Hendra and support from U.K. EPSRC grants EP/C511786/1, EP/F059396/1, and EP/G060649/1, U.K. EPSRC via the Doctoral Training Account scheme, the Royal Society, the Wolfson Foundation and Renishaw plc.

**Supporting Information Available:** Spectra recorded on gold SSV substrates. This material is available free of charge via the Internet at <http://pubs.acs.org>.

#### References and Notes

- (1) Fleischmann, M.; Hendra, P. J.; McQuillan, A. J. *Chem. Phys. Lett.* **1974**, *26*, 163.
- (2) Albrecht, M. G.; Creighton, J. A. *J. Am. Chem. Soc.* **1977**, *99*, 5215.
- (3) Jeanmarie, D. L.; Van Duyne, R. P. *J. Electroanal. Chem.* **1977**, *84*, 1.
- (4) Otto, A. *Surf. Sci.* **1980**, *92*, 145.
- (5) Otto, A.; Timper, J.; Billman, J.; Kovacs, G.; Pockrand, I. *Surf. Sci.* **1980**, *92*, L55.
- (6) Heritage, J. P.; Bergman, J. G.; Pinczuk, A.; Worlock, J. M. *Chem. Phys. Lett.* **1979**, *67*, 229.
- (7) Furtak, T. E.; Reyes, J. *Solid State Commun.* **1980**, 351.
- (8) Gersten, J. I.; Birke, R. L.; Lombardi, J. R. *Phys. Rev. Lett.* **1979**, *43*, 147.
- (9) Burstein, E.; Chen, Y. J.; Chen, C. Y.; Lundquist, S.; Tosatti, E. *Solid State Commun.* **1979**, *29*, 567.
- (10) Ueba, H. *J. Chem. Phys.* **1980**, *73*, 725.
- (11) Moskovits, M. *Rev. Mod. Phys.* **1985**, *57*, 783.
- (12) Moskovits, M. *J. Raman Spectrosc.* **2005**, *36*, 485.
- (13) Dulkeith, E.; Niedereichholz, T.; Klar, T. A.; Feldmann, J.; Plessen, G. v.; Gittins, D. I.; Mayya, K. S.; Caruso, F. *Phys. Rev. B* **2004**, *70*, 205424.
- (14) Tamitake, I.; Vasudevanpillai, B.; Mitsuru, I.; Yasuo, K.; Kazuhiro, H.; Akifumi, I.; Yukihiko, O. *J. Chem. Phys.* **2006**, *124*, 134708.
- (15) Maruyama, Y.; Futamata, M. *Chem. Phys. Lett.* **2005**, *412*, 65.
- (16) Baumberg, J. J.; Kelf, T. A.; Sugawara, Y.; Cintra, S.; Abdelsalam, M. E.; Bartlett, P. N.; Russell, A. E. *Nano Lett.* **2005**, *5*, 2262.
- (17) Cintra, S.; Abdelsalam, M. E.; Bartlett, P. N.; Baumberg, J. J.; Kelf, T. A.; Sugawara, Y.; Russell, A. E. *Faraday Discuss.* **2006**, *132*, 191.
- (18) Mahajan, S.; Abdelsalam, M.; Suguwara, Y.; Cintra, S.; Russell, A.; Baumberg, J.; Bartlett, P. *Phys. Chem. Chem. Phys.* **2007**, *9*, 104.
- (19) Abdelsalam, M. E.; Mahajan, S.; Bartlett, P. N.; Baumberg, J. J.; Russell, A. E. *J. Am. Chem. Soc.* **2007**, *129*, 7399.
- (20) Mahajan, S.; Baumberg, J.; Russell, A.; Bartlett, P. *Phys. Chem. Chem. Phys.* **2007**, *9*, 6016.
- (21) Abdelsalam, M.; Bartlett, P. N.; Russell, A. E.; Baumberg, J. J.; Calvo, E. J.; Tognalli, N. G.; Fainstein, A. *Langmuir* **2008**, *24*, 7018.
- (22) Abdelsalam, M. E.; Bartlett, P. N.; Baumberg, J. J.; Cintra, S.; Kelf, T. A.; Russell, A. E. *Electrochem. Commun.* **2005**, *7*, 740.
- (23) Mahajan, S.; Richardson, J.; Brown, T.; Bartlett, P. *J. Am. Chem. Soc.* **2008**, *130*, 15589.

- (24) Mahajan, S.; Cole, R.; Soares, B.; Pelfrey, S.; Russell, A.; Bartlett, P. N.; Baumberg, J. J. *J. Phys. Chem. C* **2009**, *113*, 9284.
- (25) Cole, R. M.; Baumberg, J. J.; Garcia de Abajo, F. J.; Mahajan, S.; Abdelsalam, M.; Bartlett, P. N. *Nano Lett.* **2007**, *7*, 2094.
- (26) Kelf, T. A.; Sugawara, Y.; Cole, R. M.; Baumberg, J. J.; Abdelsalam, M. E.; Cintra, S.; Mahajan, S.; Russell, A. E.; Bartlett, P. N. *Phys. Rev. B* **2006**, *74*, 245415.
- (27) Chen, C. Y.; Burstein, E. *Bull. Am. Phys. Soc.* **1979**, *24*, 341.
- (28) Moore, A. A.; Jacobson, M. L.; Belabas, N.; Rowlen, K. L.; Jonas, D. M. *J. Am. Chem. Soc.* **2005**, *127*, 7292.

- (29) Hong, R.; Fernandez, J. M.; Nakade, H.; Arvizo, R.; Emrick, T.; Rotello, V. M. *Chem. Commun.* **2006**, 2347.
- (30) Kassam, A.; Bremner, G.; Clark, B.; Ulibarri, G.; Lennox, R. B. *J. Am. Chem. Soc.* **2006**, *128*, 3476.
- (31) Brolo, A. G.; Irish, D. E.; Lipkowsky, J. *J. Am. Chem. Soc.* **1997**, *101*, 3906.
- (32) Timper, J.; Billman, J.; Otto, A.; Pockrand, I. *Surf. Sci.* **1980**, *101*, 348.
- JP907197B